OMTN, Volume *33*

Supplemental information

Tumor targeting and therapeutic assessments of RNA nanoparticles carrying α9-nAChR aptamer and anti-miR-21 in triple-negative breast cancers

You-Cheng Liao, Tzu-Chun Cheng, Shih-Hsin Tu, Jungshan Chang, Peixuan Guo, Li-Ching Chen, and Yuan-Soon Ho

Table S1. Sequences for construction of 3WJ RNA nanoparticles

	Sequence
A3WJ, 2'F RNA	5'-GcG uGc uGG uGc uAc-3'
B3WJ, 2'F RNA	5'-CGG UAG CAC GGG CUG UGC G-3'
C3WJ, 2'F RNA	5'-cGc AcA Gcc AGc AcG c-3'
B3WJ-Alpha9, 2'F RNA:	5'-CGG UAG CAC GGG CUG UGC G GGG AGA Auu cAA cuG ccA ucu AGG cGc uAG uAG ccu cAG cAG cAu AGu uuc Gcc Gcu AuG cAG uAA GuA cuA cAA Gcu ucu GGA cuc GGu-3'
AF647-C3WJ, 2'F RNA	5'- A647- cGc AcA Gcc AGc AcG c-3'
AF647-B3WJ, 2'F RNA	5'- A647- CGG UAG CAC GGG CUG UGC G-3'
Alpha9- C3WJ, 2'F RNA:	5'- GGG AGA Auu cAA cuG ccA ucu AGG cGc uAG uAG ccu cAG cAG cAu AGu uuc Gcc Gcu AuG cAG uAA GuA cuA cAA Gcu ucu GGA cuc GGu cGc AcA Gcc AGc AcG c-3
A3WJ -Sph1, 2'F RNA	5'-GcG uGc uGG uGc uAc cGA ucc cGc GGc cAu GGc GGc cG G GAG-3'
Sph1-anti21 DNA	5'-+G+A+T+A+A+G+C+T CTC CCG GCC GCC ATG GCC GCG GGA T-3'
Sph1-antiscr 2'F RNA	5'-cuc ccG Gcc Gcc AuG Gcc GcG GGA u-3'

*Note: Lower case c and u indicate 2'F modified.

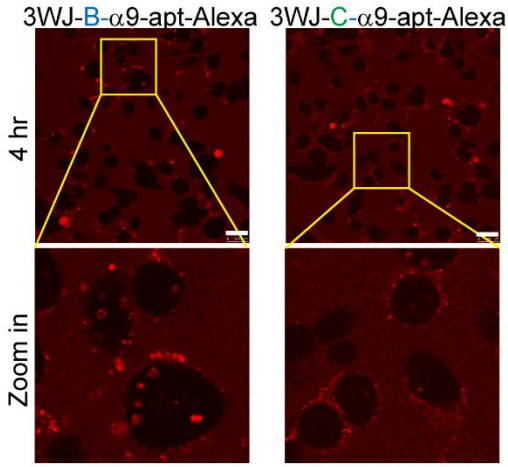

Figure S1. Live cell images of 3WJ-B-α9-apt-Alexa and 3WJ-C-α9-apt-Alexa RNA nanoparticles at 4 hours treatment in TNBC cells. Time-lapse fluorescence live cell images of MDA-MB-231 cells after treatment with 3WJ-B-α9-apt-Alexa (left) or 3WJ-C-α9-apt-Alexa (right) RNA nanoparticles. Scale bar=25 μm

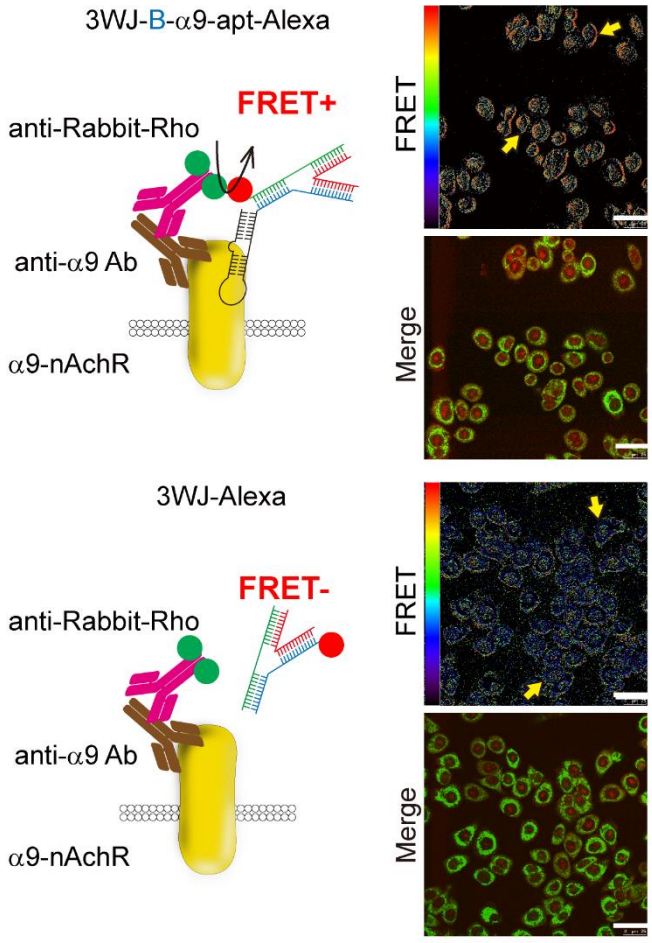

Figure S2. Confocal microscopy of specific interactions between 3WJ-B-α9-apt-Alexa RNA nanoparticles and α9-nAchR in HER2+ breast cancer cells. Confocal microscopy FRET analysis comparing the specific binding of 3WJ-B-α9-apt-Alexa and 3WJ-Alexa RNA nanoparticles (10nM, 1 hr) to α9-nAChR in SKBR3 cells. Yellow arrows indicate a positive FRET signal. The red/blue spectrum indicates the intensity of FRET efficiency. Scale bar=25 μm. Green: α9-nAchR, Red: RNA nanoparticle

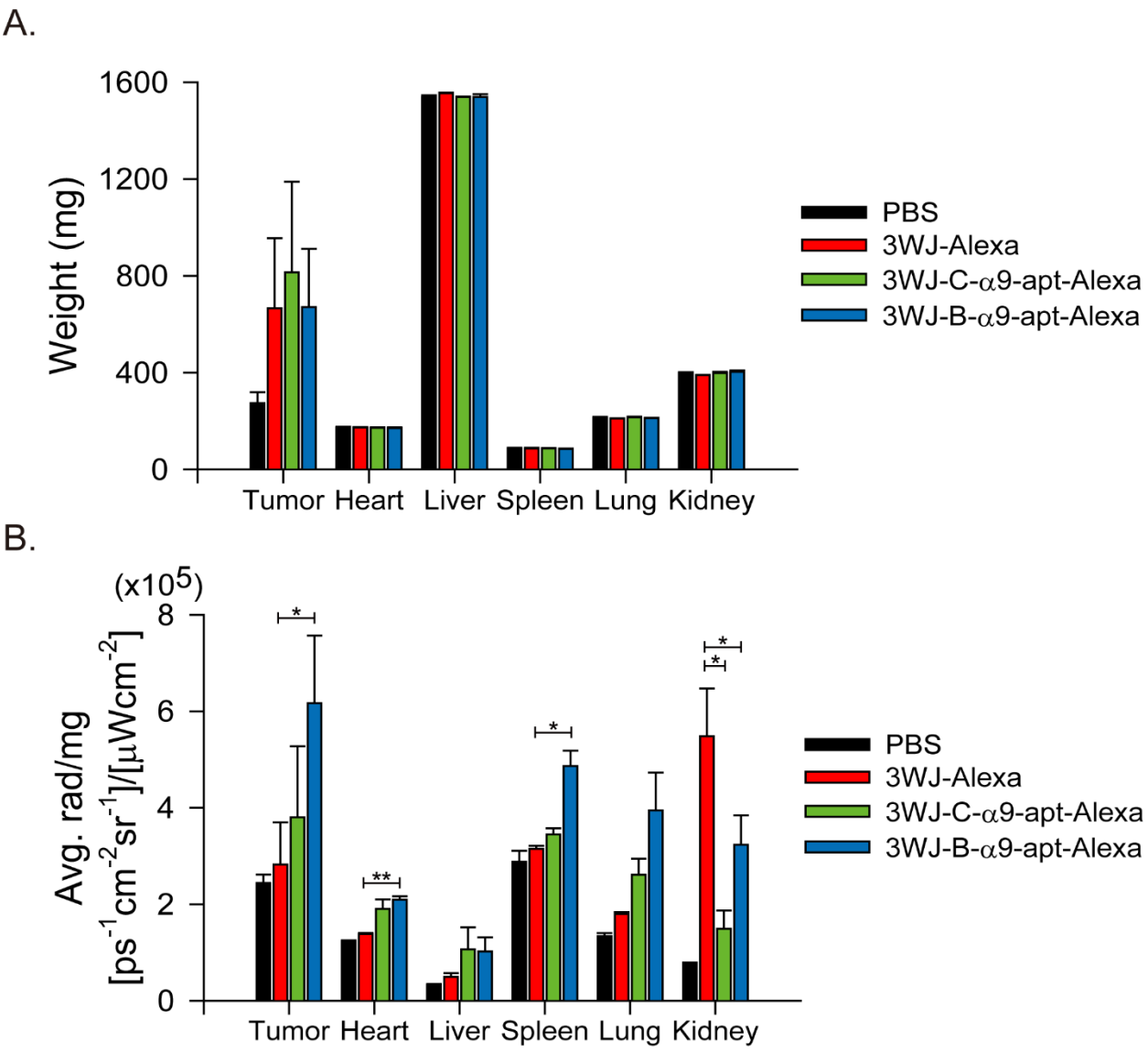

Figure S3. Quantitative analysis of the intensity of 3WJ-B-α9-apt-Alexa RNA nanoparticles in organs with normalizing against organ weight. (A) The tumor and organs weights were measured by a microbalancer after IVSIS florescent images were acquired. (B) RNA nanoparticles including 3WJ-B-α9-apt-Alexa, 3WJ-C-α9-apt-Alexa and 3WJ-Alexa uptake of organs and tumors were also calculated by dividing the average radiant efficiency (Avg) with the weights (mg) of each analyzed organ for each group of mice. (n = 3 biologically independent animals, statistics was calculated by two-tailed unpaired t-test presented as mean ± SEM, *: $p<0.05$,**: $p<0.001$)

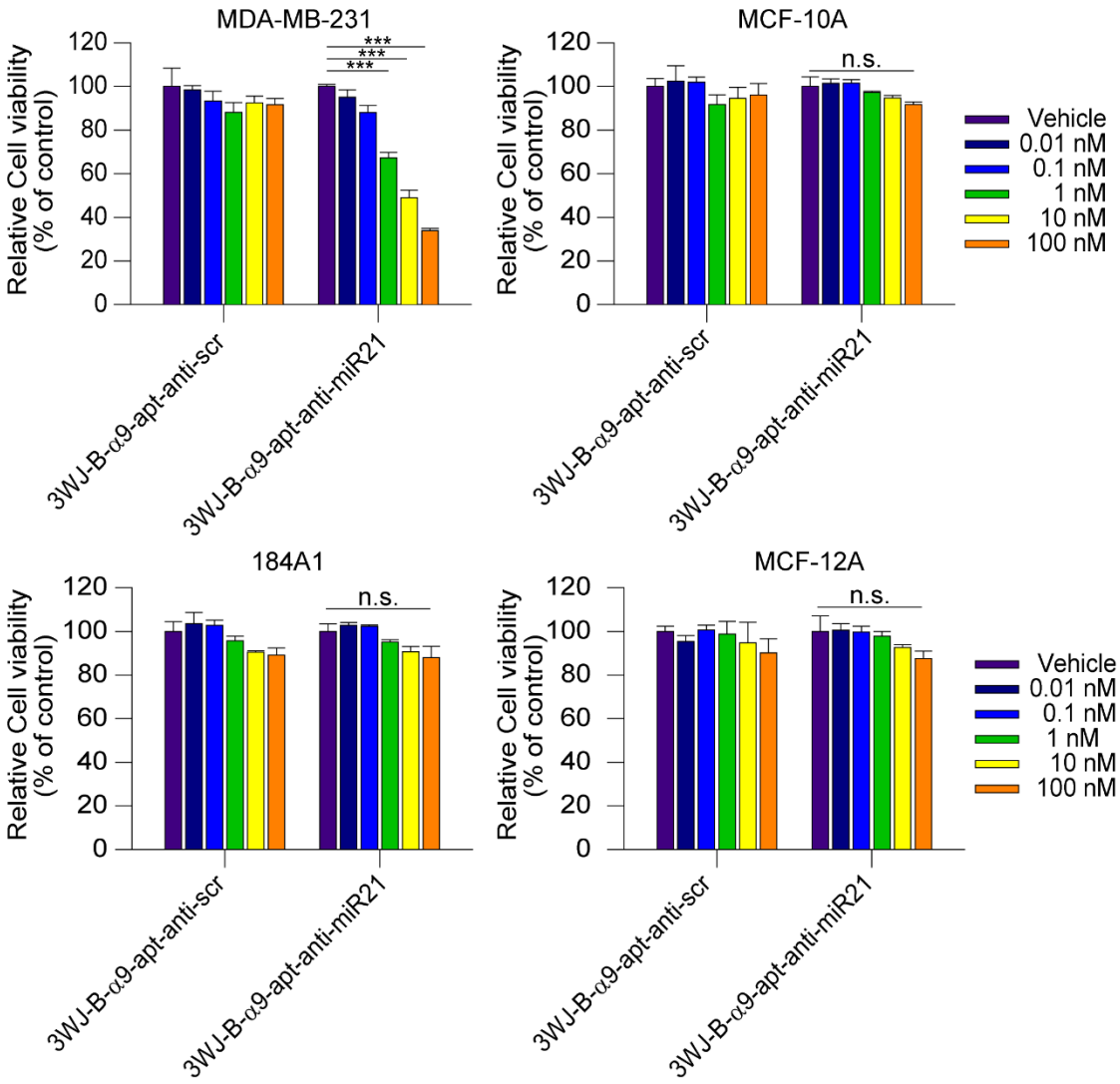

Figure S4. 3WJ-B-α9-apt-anti-miR21 RNA nanoparticles cytotoxicity evaluation in normal mammary epithelial cells. 3WJ-B-α9-apt-anti-miR21 and 3WJ-B-α9-apt-anti-scr RNA nanoparticles (0.01-100nM) treated normal mammary epithelial cells (MCF10A, MCF-12A and 184A1) and MDA-MB-231 cancer cell. Cell viability assessment was performed 48 h after drug treatment using the MTT assay. ($n = 4$ independent samples, statistics were calculated by two-tailed unpaired t-test presented as mean ± SD, $*p < 0.05$, $**p < 0.01$, $***p < 0.001$, n.s. No significance).

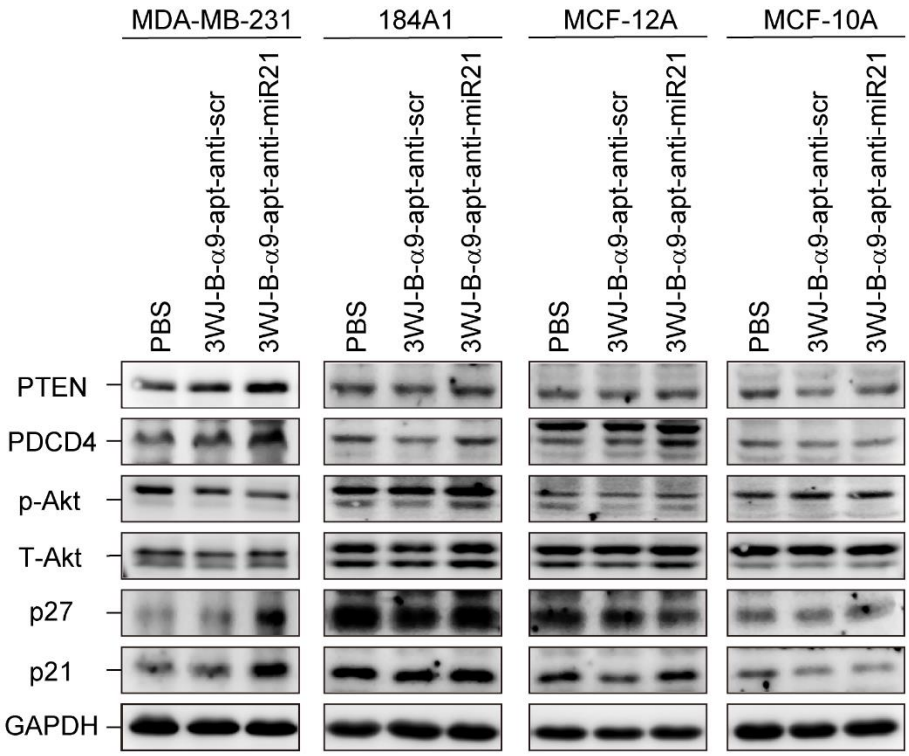

Figure S5. Protein changes induced by miR21 silencing by 3WJ-B-α9-apt-anti-miR21 RNA nanoparticles in normal breast epithelium and cancer cells. Detection of miR21 downstream targets in MCF-12A, 184 A1, and MCF-10A normal cells and MDA-MB-231 cancer cells treated with 3WJ-B-α9-apt-anti-miR21 and 3WJ-B-α9-apt-anti-scr RNA nanoparticles (10 nM, 48 hours) Protein expression including PTEN, PDCD4, p-Akt, T-Akt, p21, and p27 was detected by western blot.

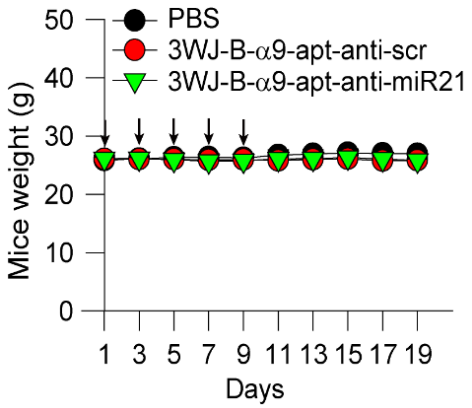

Figure S6. 3WJ-B-α9-apt-anti-miR21 RNA nanoparticles safety assessment of body weight changes in an in vivo PDX-TNBC model.